

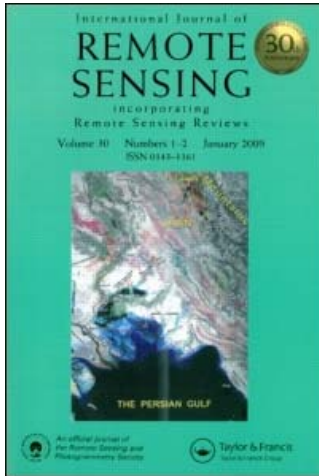
This article was downloaded by: [Kharol, Shailesh Kumar]

On: 6 February 2011

Access details: Access Details: [subscription number 933194108]

Publisher Taylor & Francis

Informa Ltd Registered in England and Wales Registered Number: 1072954 Registered office: Mortimer House, 37-41 Mortimer Street, London W1T 3JH, UK



International Journal of Remote Sensing

Publication details, including instructions for authors and subscription information:

<http://www.informaworld.com/smp/title-content=t713722504>

Forest fire monitoring and burnt area mapping using satellite data: a study over the forest region of Kerala State, India

K. V. S. Badarinath^a; A. R. Sharma^a; S. K. Kharol^a

^a Department of Space, Government of India, National Remote Sensing Agency, Balanagar, Hyderabad, India

Online publication date: 06 February 2011

To cite this Article Badarinath, K. V. S. , Sharma, A. R. and Kharol, S. K.(2011) 'Forest fire monitoring and burnt area mapping using satellite data: a study over the forest region of Kerala State, India', International Journal of Remote Sensing, 32: 1, 85 — 102

To link to this Article: DOI: 10.1080/01431160903439890

URL: <http://dx.doi.org/10.1080/01431160903439890>

PLEASE SCROLL DOWN FOR ARTICLE

Full terms and conditions of use: <http://www.informaworld.com/terms-and-conditions-of-access.pdf>

This article may be used for research, teaching and private study purposes. Any substantial or systematic reproduction, re-distribution, re-selling, loan or sub-licensing, systematic supply or distribution in any form to anyone is expressly forbidden.

The publisher does not give any warranty express or implied or make any representation that the contents will be complete or accurate or up to date. The accuracy of any instructions, formulae and drug doses should be independently verified with primary sources. The publisher shall not be liable for any loss, actions, claims, proceedings, demand or costs or damages whatsoever or howsoever caused arising directly or indirectly in connection with or arising out of the use of this material.

Forest fire monitoring and burnt area mapping using satellite data: a study over the forest region of Kerala State, India

K. V. S. BADARINATH*, A. R. SHARMA and S. K. KHAROL

Department of Space, Government of India, National Remote Sensing Agency,
Balanagar, Hyderabad 500 625, India

(Received 2 August 2008; in final form 11 March 2009)

The present study describes the night-time active forest fire detection capabilities of Defense Meteorological Satellite Program – Operational Linescan System (DMSP-OLS) satellite data over the forest region of Kerala State, India in 2004. Kerala State had a high incidence of forest fires during 2004 because of the extended dry season, with the unusual absence of intermittent rainfall from January to April. DMSP-OLS data were processed to detect active night-time forest fires over Kerala State and validated with ground data and fine-resolution Indian Remote Sensing (IRS)-P6 Advanced Wide Field Sensor (AWiFS) satellite imagery. DMSP-OLS-derived night-time fire products were compared with synchronous Moderate Resolution Imaging Spectroradiometer (MODIS)-derived daytime fire products to check for the spatial agreement and continuity of fires. To estimate the burnt areas, different atmospheric correction algorithms were applied to the IRS-P6 AWiFS dataset; these included the cosine approximation model (COST), ATCOR2 in ERDAS Imagine and the Second Simulation of a Satellite Signal in the Solar Spectrum (6S) code. Atmospheric corrections to the satellite data indicated significant improvement in burnt area estimates. The results of the study suggest a good correlation between AWiFS data-derived burnt areas, DMSP-OLS-derived fire counts and MODIS-derived fire products. The fire occurrences derived from DMSP-OLS and MODIS data were validated with field records on fire occurrences over the study area.

1. Introduction

Forest fires occurring in remote and inaccessible forest areas make it difficult to monitor using conventional ground-based methods. In this context, remote sensing data provide consistent and unbiased observations of fire activity over large regions (Kiran Chand *et al.* 2006, Badarinath *et al.* 2007). Fire is a prominent disturbance factor and is an agent of environmental change with local to regional impacts on land use, productivity, carrying capacity and biodiversity, and regional to global impacts on hydrological, biogeochemical and atmospheric processes (Roy *et al.* 2005). The monitoring and management of forest fires is very important in tropical countries such as India, where forests are prone to fires annually causing adverse ecological, economic and social impacts (Kiran Chand *et al.* 2006). Earlier studies on the impacts of tropical wild fires on the environment have indicated high organic carbon emissions (Hao *et al.* 1996, Fearnside 2000), emissions of large amounts of trace gases and

*Corresponding author. Email: badrinath_kvs@nrsc.gov.in

aerosol particles (Crutzen and Andreae 1990, Govaerts *et al.* 2002, French *et al.* 2003), black carbon (Dwyer *et al.* 1998) and the release of almost 100 million tonnes of smoke aerosols into the atmosphere as a result of biomass burning (Hao and Liu 1994). These submicrometre smoke aerosols play a major role on the radiation balance of the Earth-atmospheric system (Kaufman *et al.* 1998a). There is also widespread concern about the loss of biodiversity, the effects on atmospheric chemistry and the increase in surface albedo and water runoff due to biomass burning (Reid *et al.* 2005). Apart from the natural fires, the major sources of forest fires in India are anthropogenic, and include shifting cultivation practices, controlled burning, deforestation and firewood burning. The conventional methods of fire protection cover an elaborate network of fire lines, fire watch towers, block lines and manual fire control systems that at times becomes difficult in practice because of a lack of manpower, resource constraints and time-effective control mechanisms. However, application of remotely sensed data from spaceborne sensors on different platforms and the use of geographic information systems (GIS) are capable of addressing the problem with scientific and technical strength in a time- and cost-effective manner. Satellite remote sensing can provide information on the occurrence of fires, and can indicate the magnitude and temporal dynamics of forest cover change through deforestation by burning events.

The use of remote sensing in monitoring forest fires is well known. Dozier (1981) used the sensitivity of middle-infrared (mid-IR) (3.7 μm) channel radiance of the Advanced Very High Resolution Radiometer (AVHRR) to identify hot objects that may cover only a small fraction of a pixel. Matson *et al.* (1984, 1987) worked on the National Oceanic and Atmospheric Administration (NOAA) series of satellites in detecting forest fires. In more recent studies, information given by the thermal bands of the Moderate Resolution Imaging Spectroradiometer (MODIS) onboard Terra and Aqua satellites has been used in an effective way to detect active forest fires. An enhanced contextual fire detection algorithm using MODIS version 4 fire products (Giglio *et al.* 2003) uses the brightness temperatures at 4 and 11 μm for detecting fires. The algorithm also includes processing steps for the removal of cloud cover and water bodies, the identification of potential fire pixels, background characterization and deletion of hot targets thereby reducing false alarms caused by various factors. Data from the Defense Meteorological Satellite Program (DMSP) Operational Linescan System (OLS) have the unique capability of sensing night-time lights even in dim light and cloud cover, thus presenting scope for accurate monitoring of near-real-time fire events.

In Earth observations, the atmosphere has an influence on the visible and IR radiation that is strong enough to modify the reflected electromagnetic signal and at-target reflectance (Liang *et al.* 2001, Vermote *et al.* 2002). Scattering of solar irradiance by atmospheric molecules and aerosols generates the path radiance, which increases the apparent surface reflectance over dark surfaces, while absorption by aerosols and other molecules in the atmosphere causes loss of brightness to the scene, as recorded by the satellite sensor (Lu *et al.* 2002, Masek *et al.* 2006). In particular, both atmospheric scattering and absorption are enhanced at shorter wavelengths where the particle size is similar to the radiation wavelength. The adjacency effect (AE) is an interesting physical phenomenon caused by atmospheric crosstalk between fields of different surface reflectance (Richter *et al.* 2006). The AE reduces the apparent surface contrast by decreasing the top of the atmosphere (TOA) radiance over bright pixels and increasing the brightness of the dark pixels (Lyapustin and Kaufman 2001). The AE causes a blurring effect and reduces the

contrast of an image, and is therefore important in remote sensing applications. Significant errors in retrieved surface reflectance at the red wavelength due to the AE can be up to 0.07 at a viewing zenith angle of 53.1° even at 1 km resolution (Lyapustin and Kaufman 2001). The adjacency correction is small for coarse-resolution sensors but becomes highly significant for high spatial resolution sensors (Sei 2007). Minimizing atmospheric effects in remotely sensed imagery includes the use of physically based radiative transfer models and image-based atmospheric correction models. Radiative transfer models require many simulations and many *in situ* input parameters (Lu *et al.* 2002, Vermote and Saleous 2006). These radiative transfer models include the Second Simulation of a Satellite Signal in the Solar Spectrum (6S) radiative transfer code (Vermote *et al.* 1997), the LOW resolution TRANsmission (LOWTRAN) model (Kneizys *et al.* 1988), the MODerate spectral resolution atmospheric TRANsmittance (MODTRAN) algorithm (Berk *et al.* 1989), the Simulation of a Satellite Signal in the Solar Spectrum (5S) code (Tanre *et al.* 1990) and the Simplified Method for Atmospheric Correction (SMAC; Rahman and Dedieu 1994). Of the various radiative transfer models, the 6S radiative transfer code is the most sophisticated and highly accurate (Vermote *et al.* 1997, Tachiri 2005). Several researchers have conducted studies on the effectiveness of the 6S code for atmospheric corrections. For example, Stroeve and Steffen (1997) tested the potential of the 6S code for atmospheric corrections of visible and near-infrared (NIR) channels in AVHRR data in polar regions and found significant improvements in albedo after atmospheric corrections. Zhao *et al.* (2001) used the 6S code for atmospheric and spectral corrections and estimating surface albedo from Landsat Thematic Mapper (TM) data; they found nearly 6% improvement in surface albedo after atmospheric corrections. Tachiri (2005) used the 6S code for correcting normalized difference vegetation index (NDVI) images from NOAA/AVHRR data in northern Kenya and found a considerable increase in the range of NDVI after atmospheric corrections, with the characteristic that the greater the NDVI the larger was the atmospheric effect. Vermote and Saleous (2006) also demonstrated the utility of the 6S code for atmospheric corrections for MODIS visible to mid-IR land surface data.

The image-based atmospheric correction models do not require any *in situ* atmospheric information and include dark object subtraction (DOS), the cosine approximation model (COST) and the pseudo-invariant object method. Inputs required to implement these models are mainly based on image parameters and the data header file, which provides information on image acquisition, sun angle and calibration coefficients.

The present study investigated the potential use of DMSP-OLS data in detecting night-time active fires in Kerala State, India, during 2004. The forests of Kerala experienced more fire episodes than usual during 2004 because of drought conditions and in this study we tried to enumerate the burnt area in terms of the total number of fire episodes. Atmospheric correction to the Indian Remote Sensing (IRS)-P6 Advanced Wide Field Sensor (AWiFS) satellite data was performed using different algorithms and the effect of each algorithm was analysed for burnt area mapping using satellite data.

2. Study area

Figure 1 shows the location map of the study area with forest division boundaries. Kerala is one of the smallest states of India, lying in the extreme southwest of the peninsula and extending over a distance of 560 km along the west coast. The word 'Kerala' means Land

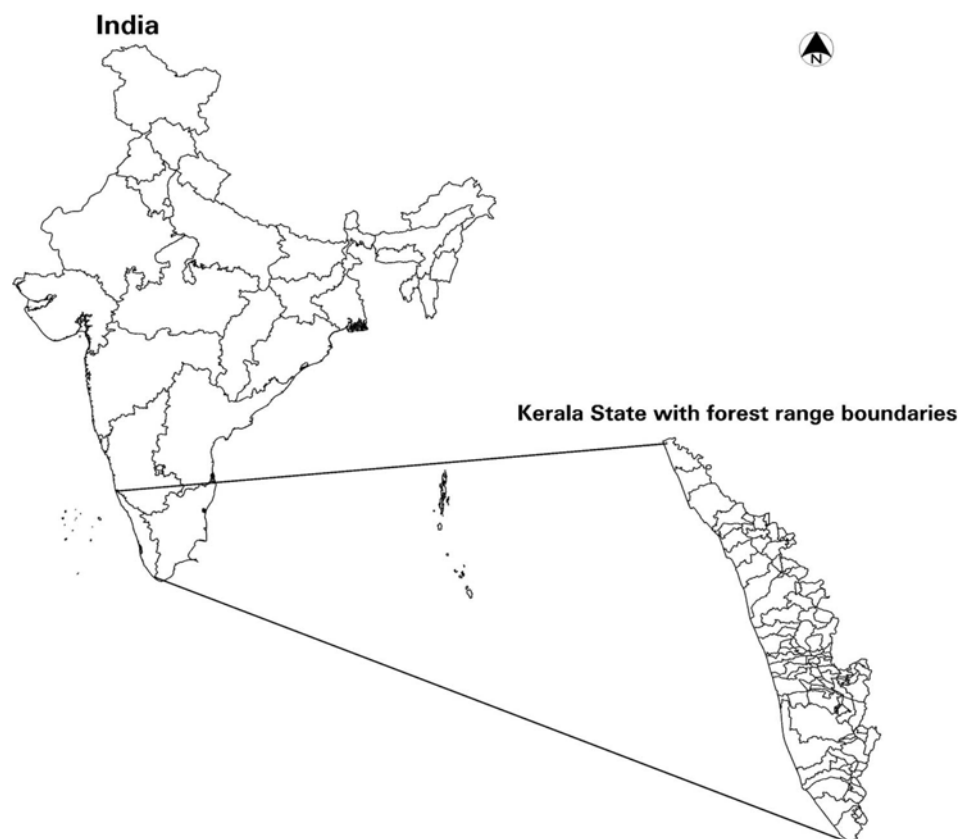


Figure 1. Location map of the study area with forest range boundaries.

of Coconut in vernacular. The east–west land width varies from 15 to 120 km. Kerala lies between 8.2° and 12.8° N and 74.8° and 77.5° E, covering an area of $38\,864\text{ km}^2$ (figure 1). The Western Ghats form a mountain wall extending north–south with a few breaks in the chain, the most prominent being the Palakkad gap, which is 24 km wide and as low as 300 m a.s.l., considered as originating from tectonic and erosional processes. The mountains are plateau remnants of two or three altitudinal ranges, at approximately 1800, 1200 and 600 m, called the Plantation surfaces. These plateau remnants are considered to be the result of periodic uplift of this part of the Western Ghats. The average height of the Western Ghats in Kerala is about 950 m but it rises from the sea level in the coast and up to the order of 2695 m at Anaimudi, the highest peak in peninsular India. The coastal plain has a few scattered hillocks with rocky cliffs. The plains are dotted by 34 kayals (lagoon or estuary), facilitating inland navigation. Vembanad Lake, south of Cochin, is the largest (205 km^2), followed by Ashtamudi kayal further south. Kerala State, located in the Western Ghats, is one of the most important biodiversity hotspots and harbours a range of diverse flora. Kerala has a total forest cover of $10\,334\text{ km}^2$ (26.59%), of which 8454 and 1880 km^2 are dense and open forests, respectively. Kerala, with a per capita forest of 0.04 ha, one of the lowest, exhibits a certain level of protection. This is clearly expressed by its large number of unique and endemic flora. It has been observed that Kerala State exhibits biodiversity on all levels of genetic, species and habitat diversity; for example, *Cymbopogon flexuosus*, the ginger

grass in the Western Ghats, is said to have as many as 3000 variants with respect to essential oil constituents. Of the 25 Dalbergia species, seven are found in Kerala.

3. Datasets and methodology

DMSP-OLS and Terra MODIS satellite data sets (at 250, 500 and 1000 m) for 18 March 2004 were used in generating fire products and for comparison purposes. High spatial resolution data sets of IRS-P6 AWiFS at 56-m spatial resolution for 19 March 2004 were used for validating the DMSP-OLS-derived fires by visibly locating fires/plumes and with the burnt scar assessment.

3.1 Description of sensors

3.1.1 DMSP. DMSP operates F14, F15 and F16 satellites in Sun-synchronous orbits. The night-time overpasses of these satellites range from about 7 pm to 10 pm local time. With a 3000 km swath width, portions of India are observed in two or three OLS orbital passes from each of the satellites. The OLS is an oscillating scan radiometer with two spectral bands. The visible band straddles the visible and NIR portion of the spectrum (0.5–0.9 μm). The thermal band covers the 10.5–12.5 μm region. DMSP-OLS was basically designed for global observation of cloud cover. At night, the visible band is intensified with a photomultiplier tube (PMT) to permit detection of clouds illuminated by moonlight (Elvidge *et al.* 2001). The high sensitivity of the OLS at night permits the measurement of radiances down to $10^{-9} \text{ W cm}^{-2} \text{ sr}^{-1}$. Fires present at the Earth's surface at the time of the night-time overpass of the DMSP are readily detected in the visible band data. By contrast, fires rarely show up as hot spots in the OLS thermal band data. The OLS data are acquired in two spatial resolution modes: 'fine' data at a nominal ground sample distance (GSD) of 0.5 km and 'smoothed' data at a GSD of 2.7 km. The near-real-time (≥ 3 h old) night-time DMSP-OLS data of the Indian region used in this study were provided by an automated subscription service from the NOAA National Geophysical Data Center (NGDC) in Boulder, CO, USA.

3.1.2 MODIS. MODIS is one of the five sensors onboard Terra/Aqua satellites with 36 spectral bands and it acquires data at three different spatial resolutions, 250 (bands 1 and 2), 500 (bands 3–7) and 1000 m (bands 8–36), covering the visible, NIR, shortwave infrared (SWIR) and thermal-infrared (TIR) regions of the electromagnetic spectrum.

3.1.3 AWiFS. The AWiFS operates in four spectral bands in the green (0.52–0.59 μm), red (0.62–0.68 μm), NIR (0.77–0.86 μm) and SWIR (1.55–1.70 μm) at 56-m spatial resolution. It has a swath width of 740 km and a revisit period of 5 days.

3.2 Description of algorithms for DMSP fire generation

Figure 2 shows the flow diagram of the procedure implemented in deriving OLS fire products. Fire detection using DMSP-OLS night-time data is based on the identification of lights outside the set of known persistent (stable) lighting sources. A stable lights database is generated using a time series of OLS data. The basic procedure used to generate the stable lights image has been described by Elvidge *et al.* (1997). The stable lights database is used as a mask, which is applied to the incoming data stream. Lights found on land, but outside the stable lights mask, are possible fires. The initial steps for generating an OLS fire product, including the identification of lights and

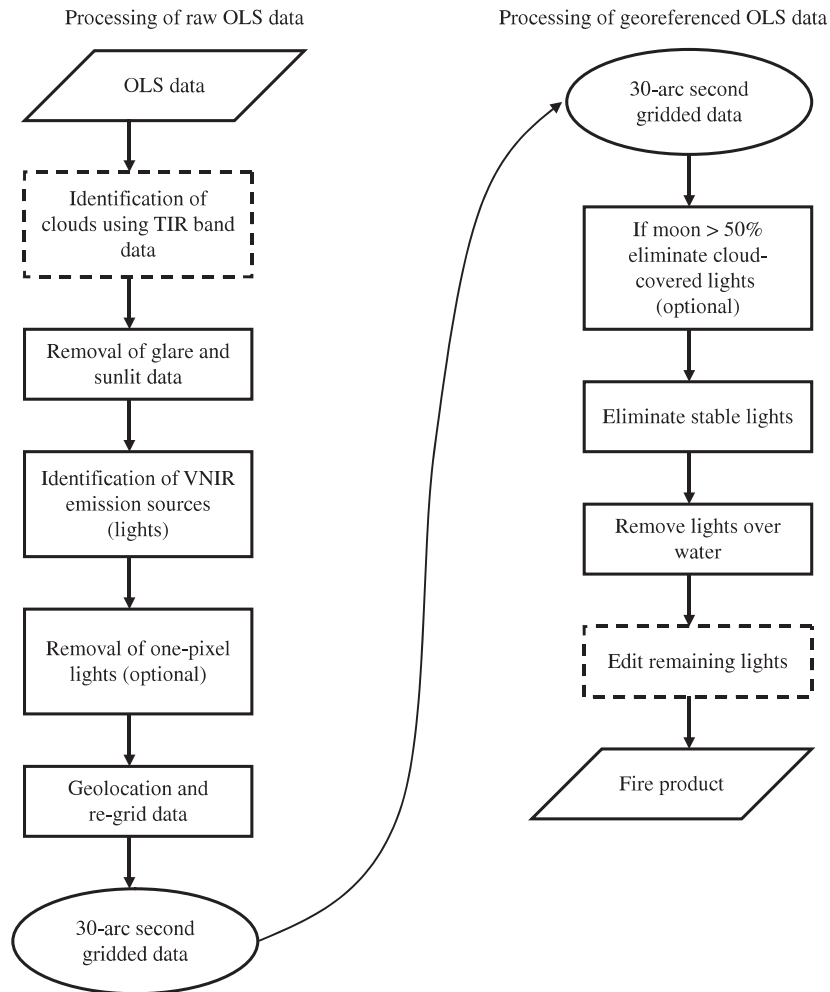


Figure 2. Flow chart of procedure used to derive DMSP-OLS fire products.

clouds, missing data and poor scan lines, plus geolocation, are fully automated. These procedures are described in Elvidge *et al.* (2001). The light detection algorithm settings are tightened during full-moon nights to reduce the number of light detections from moonlit clouds. Pixel identities (e.g. lights, clouds, clouds with lights and missing scan lines) are marked in a flag file that overlays the OLS image data. The light detections can be filtered to remove light detections that coincide with clouds. This is particularly useful on nights with strong moonlight. The light detections are then filtered based on the stable lights mask and a mask for water bodies. As a final step the remaining lights are overlaid with the stable lights data and the thermal band image and visually reviewed to identify and remove light sources that are not from fires. This may include poor scan lines, lightning, city lights not fully removed, or heavily lit clouds. After the final editing of the DMSP-OLS fires image, fires that fall within the forest regions of the study area are extracted using a forest mask image to eliminate additional lights that are not part of the forest regions.

3.2.1 MODIS fire algorithm. Fire images were generated from MODIS using the revised version 4 contextual algorithm given by Giglio *et al.* (2003), which is based on the original MODIS fire detection algorithm (Kaufman *et al.* 1998b). The algorithm uses brightness temperatures derived from MODIS 4 and 11 μm channels, denoted by T_4 and T_{11} , respectively. The MODIS instrument has two 4 μm channels, numbered 21 and 22, with band widths of 3.929 to 3.989 μm (3.959 central wavelength), respectively; these are used in the detection algorithm to derive T_4 . Channel 21 saturates at nearly 500 K and channel 22 saturates at 331 K. As the low-saturation channel (22) is less noisy and has less quantization error, T_4 is derived from channel 22 whenever possible. However, when channel 22 saturates or has missing data, it has been replaced by channel 21 to derive T_4 . Brightness temperature T_{11} was computed from the 11 μm channel (channel 31), which saturates at approximately 400 K. The brightness temperature computed from channel 32 is denoted T_{12} and was used in cloud and water masking.

The 2500 m resolution red and NIR channels (channels 1 and 2), aggregated to 1 km, was used to reject false alarms and masking clouds. Reflectances of the red and NIR bands are denoted by $\rho_{0.65}$ and $\rho_{0.86}$, respectively. The MODIS contextual algorithm includes cloud and water masking, identification of potential fire pixels to eliminate obvious non-fire pixels, background characterization, contextual threshold tests to confirm fire among the potential fire pixels and sunglint, desert boundary and coastal false alarm rejection. It examines each pixel of the MODIS swath and assigns it to one of the following classes: missing data, cloud, water, non-fire, fire or unknown. A detailed description of the algorithm has been presented previously (Giglio *et al.* 2003).

3.3 Atmospheric corrections

Quantitative modelling of the interaction between solar radiation and the surface/atmosphere system is indispensable for surface reflectance retrieval (Guanter *et al.* 2007a,b). The digital number (DN) of the satellite data was converted to spectral radiance (L_i) using prelaunch calibration coefficients and then the TOA reflectance ($\rho(\lambda_i)$) for each spectral band (i) was computed by converting spectral radiance to reflectance as

$$\rho_{\lambda_i} = \frac{\pi L_i d^2}{E_0 \cos \theta} \quad (1)$$

where d is the Earth–Sun distance, E_0 is the extraterrestrial solar irradiance and θ is the solar zenith angle. Further atmospheric corrections to the satellite data were carried out using the following algorithms individually.

3.3.1 The COST model. The COST model was developed to account for the multiplicative effects of atmospheric scattering and absorption (Chavez 1996). In this model, the cosine function of the solar zenith angle (θ) is used to approximate atmospheric transmittance (T_λ^θ), to first order (Wu *et al.* 2005). The equation for retrieving surface reflectance can be expressed as:

$$\rho_\lambda(x, y) = \frac{\pi}{T_\lambda^v} \frac{L_\lambda^s(x, y) - L_\lambda^p}{T_\lambda^s D E_\lambda^0 \cos(\theta^s) + E_\lambda^d} \quad (2)$$

where $\rho_\lambda(x, y)$ is the spectral reflectance at the surface for an image pixel at column x and row y , E_λ^0 is the extraterrestrial solar spectral irradiance for wavelength λ at the mean Earth–Sun distance, D is a correction factor for the Earth–Sun distance, E_λ^d ($\text{W m}^{-2} \mu\text{m}^{-1}$) is the downwelling atmosphere-scattered solar spectral irradiance, L_λ^s ($\text{W m}^{-2} \text{sr}^{-1} \mu\text{m}^{-1}$) is the total spectral at-sensor radiance, L_λ^p ($\text{W m}^{-2} \text{sr}^{-1} \mu\text{m}^{-1}$) is the upwelling atmosphere-scattered spectral radiance, T_λ^s and T_λ^v are the atmospheric spectral transmittances at λ in solar path with a solar zenith angle θ^s and in view path with a satellite view angle θ^v , respectively.

3.3.2 ATCOR model. The ATCOR2 module is commercially available for atmospheric correction in ERDAS Imagine software (ERDAS, Inc., Norcross, GA, USA; Stefanov *et al.* 2001). This module has a large database containing the results of radiative transfer calculations based on the MODTRAN-4 code as an integral part covering a wide range of weather conditions, sun angles and ground elevations. The ATCOR2 module requires input parameters on the solar zenith angle, date and time of image acquisition, sensor type, visibility and aerosol type. Details on the ATCOR2 model are described elsewhere (www.op.dlr.de/atcor/).

3.3.3 6S code implementation. The 6S code predicts the reflectance of the objects at the TOA using information about the surface reflectance and atmospheric conditions (Vermote *et al.* 1997). The surface reflectance free from atmospheric effect is computed as (Mahiny and Turner 2007):

$$\text{Ref} = (A\rho + B) / \{1 + [Y(A\rho + B)]\} \quad (3)$$

where $A = 1/\alpha\beta$, $B = -\rho/\beta$ (α is the global gas transmittance, β is the total scattering transmittance), Y is the spherical albedo and ρ is the atmospheric reflectance. To run the 6S model several inputs parameters are required, including the solar zenith and azimuth angles, satellite zenith and azimuth angles, date and time of image acquisition, type of sensor, water vapour, ozone, aerosol optical depth (AOD), aerosol model, target elevation and sensor elevation.

The input parameters on the solar zenith and azimuth angles, satellite zenith and azimuth angles, date and time of image acquisition required for the 6S model were extracted from the AWiFS dataset. AOD data at 550 nm from MOD04 Level-2 at 10×10 km resolution (<http://ladsweb.nascom.nasa.gov/data>), water vapour from MOD08_M3.005 products (<http://g0dup05u.ecs.nasa.gov/Giovanni/>) and columnar ozone data from L3_Ozone_OMI products (<ftp://toms.gsfc.nasa.gov/pub/omi/data/ozone>) were also used in the 6S model. Correction for the AE involves inverting the linear combination of reflectances to isolate the reflectance of the target pixel (Guanter *et al.* 2007b). The formulation proposed by Vermote *et al.* (1997) was used, weighting the strength of the AE by the ratio of diffuse to direct ground-to-sensor transmittance:

$$\rho_s = \rho_s^\mu + \frac{t_d}{e^{-\tau/\mu_v}} [\rho_s^\mu - \bar{\rho}] \quad (4)$$

where ρ_s^μ is the surface reflectance before the adjacency treatment, ρ_s is the final surface reflectance, the output of the complete atmospheric correction algorithm, t_d is the diffuse transmittance, τ is the total optical thickness, μ_v is the cosine of the view zenith angle and $\bar{\rho}$ is the average of the environment reflectance.

3.4 Burnt area mapping

To estimate the recently burnt area due to forest fires, the supervised classification technique was applied on uncorrected and atmospherically corrected IRS-P6 AWiFS satellite images. The atmospheric correction methods used were the COST model, the ATCOR model and the 6S code. The process used for the corrected images was identical to that used for the uncorrected images. The maximum likelihood classifier was chosen to allocate each pixel to its nearest class. The separability and contingency analysis of the training sites indicated that all classes were completely distinct and more than 97% of the pixels in the training sites were correctly classified. DMSP-derived fire counts and burnt areas estimated from AWiFS data were verified with field information provided by the State forest department. Daily fire products derived from DMSP-OLS data were compared with the visible and thermal data sets of AWiFS and MODIS to estimate the spatial agreement between the information obtained from the different satellite data.

4. Results and discussion

Figure 3(a) and 3(b) shows the first and second fortnightly composites, respectively, of DMSP-OLS-derived night-time forest fires during March 2004. These figures reveal that during this period Kerala State experienced intense forest fire episodes. The high

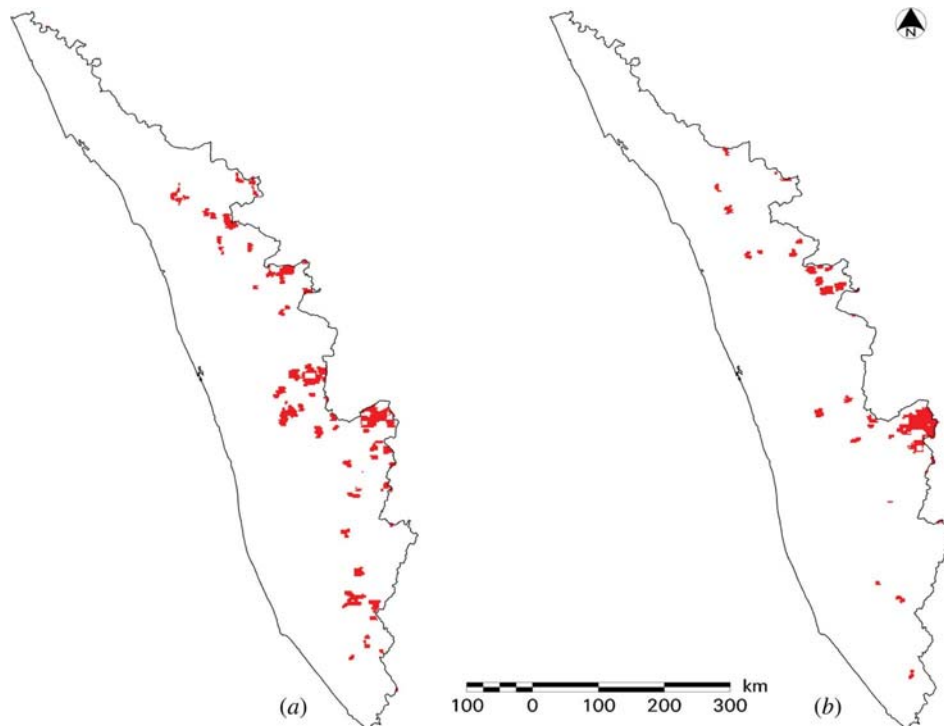


Figure 3. (a) First and (b) second fortnightly composites of DMSP-OLS-derived night-time forest fires in Kerala during March 2004.

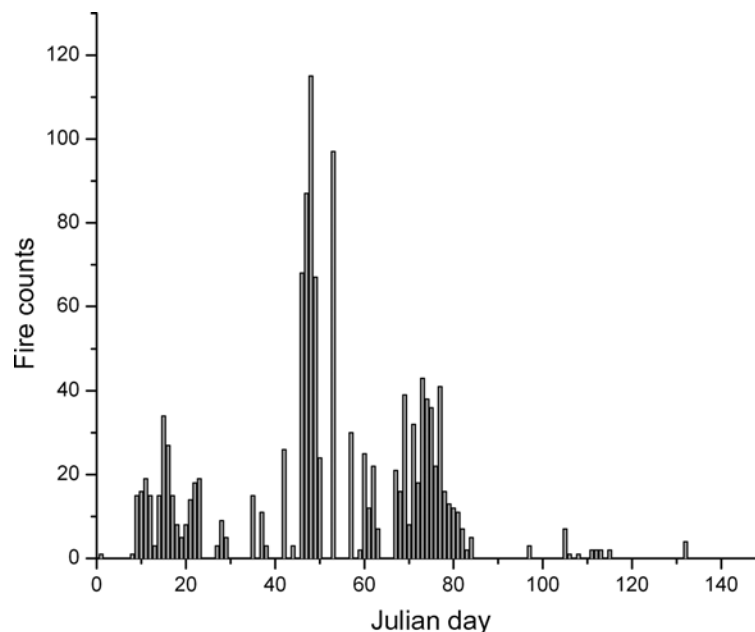


Figure 4. DMSP-OLS-derived number of fire counts over Kerala State plotted against the Julian day of the year 2004.

incidence of fires in Kerala State in 2004 has been attributed to decreased rainfall during January to March and sustained high temperatures compared to normal years.

Figure 4 shows the Julian day (the sequential day count of the days of a year, reckoned consecutively from the first day of January) variation of forest fire counts derived from DMSP-OLS night-time satellite datasets during January to May 2004 over Kerala State. It is clear from figure 4 that the fires started in January and progressed to May with a peak occurrence during February–March. The fires occurred predominantly in dry deciduous forest regions and grasslands because of the dry fuel load (Kiran Chand *et al.* 2006). Figure 4 indicates that the highest number of fire episodes took place from 14 to 20 February, with the fire count reaching up to 115 episodes per day. The distribution and occurrence of forest fires were matched with fire records of the State forest department and local information from other sources.

To understand the spatial distribution of the forest fires, we compared MODIS- and DMSP-OLS-derived active fire locations over the study area on 18 March 2004. Figure 5 shows a comparative analysis of the night-time DMSP-OLS- and daytime AQUA-MODIS-derived fire products of 18 March 2004 over the study area. A false colour composite (FCC) of MODIS 500 m data (figure 5(b)), generated by assigning a red colour to the SWIR band ($1.24 \mu\text{m}$), green to the green band ($0.555 \mu\text{m}$) and blue to the blue band ($0.469 \mu\text{m}$), clearly shows the smoke plumes emanating from active fire locations over the study area. Similarly, the MODIS FCC of 500 m data (figure 5(c)), generated by assigning a red colour to the SWIR band ($1.64 \mu\text{m}$), green to SWIR ($1.24 \mu\text{m}$) and blue to green ($0.555 \mu\text{m}$), shows the active fire pixels in red. Active fire pixels of MODIS (figure 5(e)) and DMSP (figure 5(f)) show good spatial agreement in fire occurrence, indicating the continuation of fires from daytime to night-time in

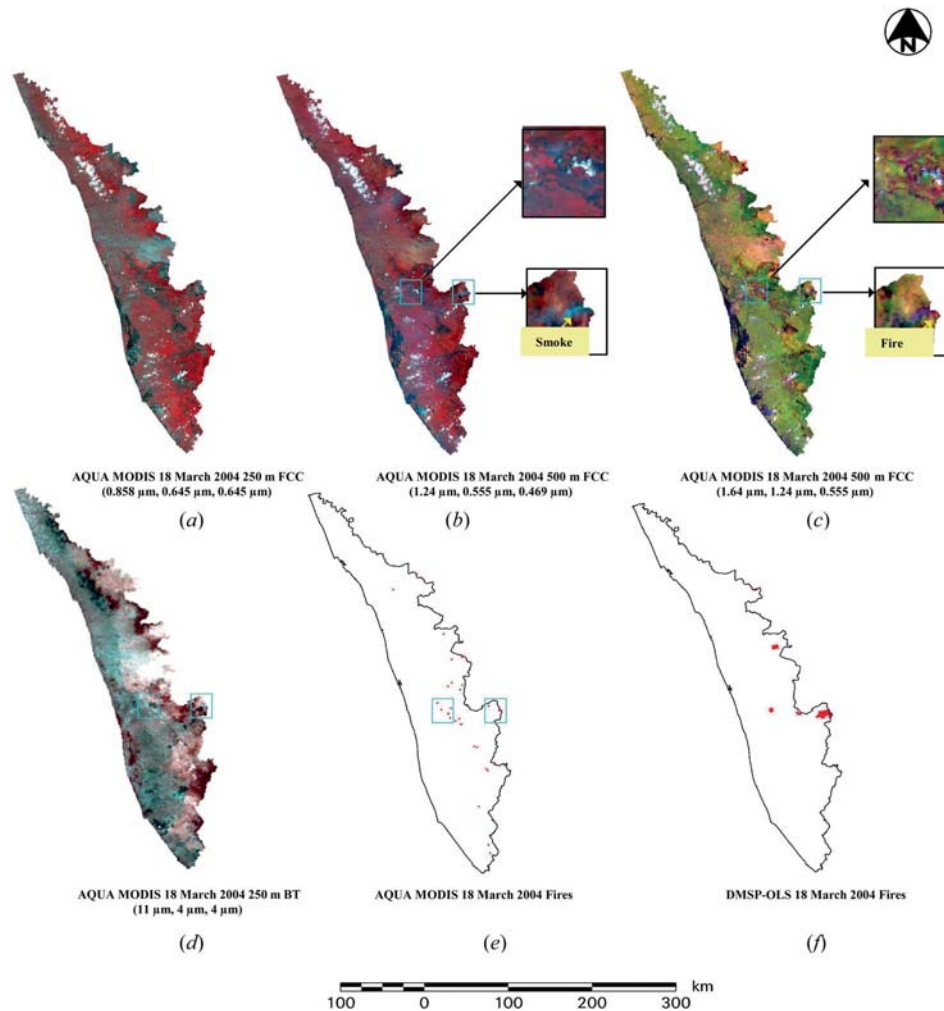


Figure 5. Comparison of DMSP-OLS-derived fires with MODIS-derived fires on 18 March 2004. (a) FCC of MODIS 250 m data (0.858, 0.645 and 0.645 μm); (b) FCC of MODIS 500 m data (1.24, 0.555 and 0.469 μm) showing plumes emanating from fires; (c) FCC of MODIS 500 m data (1.64, 1.24 and 0.555 μm) showing active fires as red-coloured pixels; (d) FCC of MODIS 1 km brightness temperature data (11, 4 and 4 μm); (e) active fire locations derived from AQUA MODIS on 18 March 2004; (f) active fire locations derived from DMSP-OLS on 18 March 2004.

certain areas. Over the Indian region, the fires are short lived, that is less than 1 h in most cases, and they occur in small patches (< 10 ha) over large regions. This makes one-to-one comparison difficult with data from different fire products (Kiran Chand *et al.* 2006, Prasad *et al.* 2008).

Burnt areas estimated from AWiFS data were validated by overlaying DMSP-OLS-derived fires of 18 March 2004 with IRS-P6 AWiFS data of 19 March 2004. The fires observed in DMSP-OLS were found to fall within the burnt area patches observed in AWiFS data of the subsequent day (figure 6). Figure 7 shows the IRS-P6 AWiFS FCC (a) before atmospheric correction and (b) after atmospheric

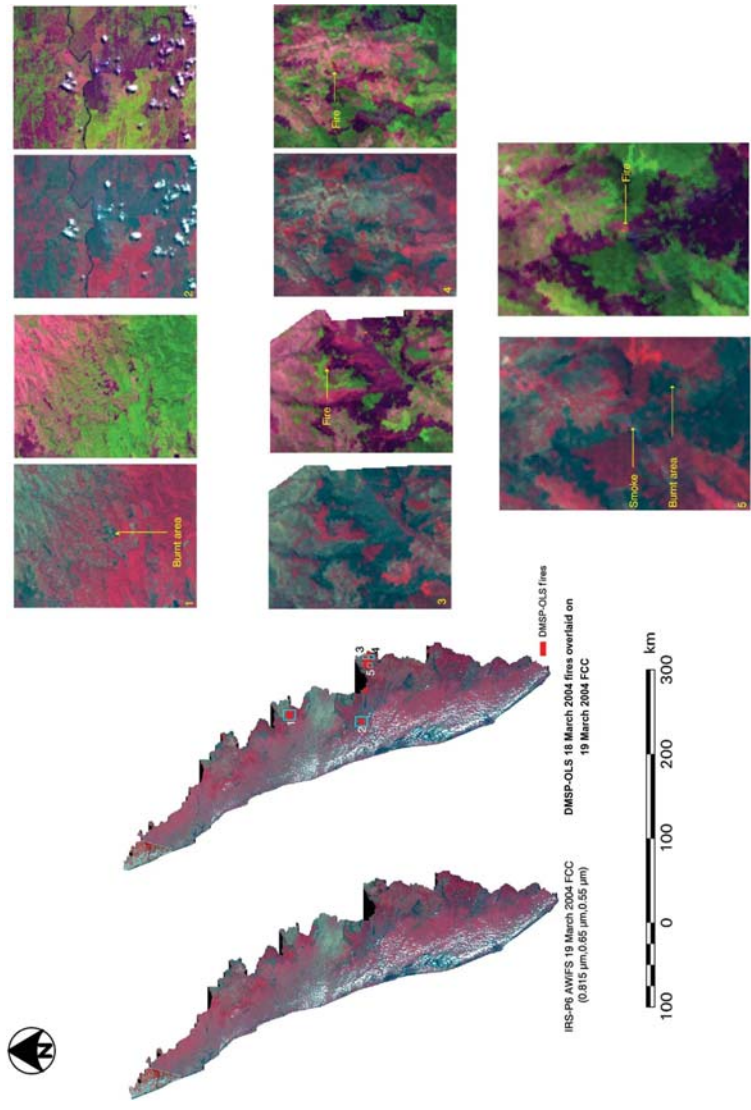


Figure 6. FCCs of AWiFS data (red to 0.816 μm , green to 0.65 μm , blue to 0.55 μm and red to 1.625 μm , green to 0.816 μm , blue to 0.65 μm) of 19 March 2004 overlaid with DMSP-OLS-derived fires of 18 March 2004. The small square images on the right-hand side are enlarged portions of the square boxes marked on the left-hand side, depicting forest fires.

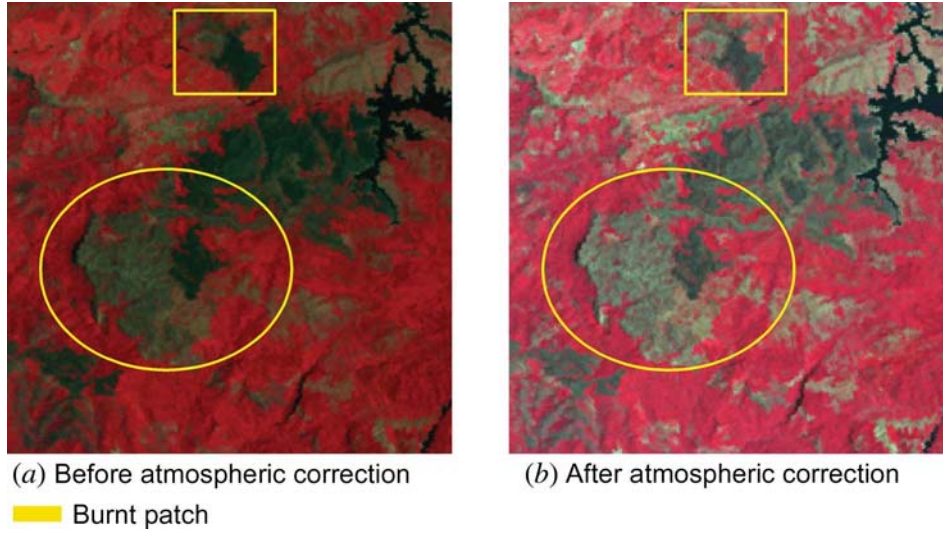


Figure 7. FCCs of AWiFS data of 19 March 2004 (a) before and (b) after atmospheric correction.

correction on 19 March 2004 over part of Kerala State. In figure 7(a), the areas marked on the image show deciduous forests that were appearing as burnt patches before atmospheric correction. The atmospheric correction to the AWiFS data using the 6S code improved the discrimination between deciduous forest and burnt areas over the study region. Visual comparison of the raw and atmospherically corrected images showed that the overall representation of features and levels of contrast was better in the corrected images (Sharma *et al.* 2009). Spectral profiles for distinctive objects were also found to match with their spectral reference library counterparts well.

To estimate the separability between various land use features before and after atmospheric corrections, transformed divergence distances were calculated using the following equation (5):

$$TD(i,j) = 2 \left[1 - \exp\left(\frac{-D(i,j)}{8}\right) \right] \quad (5)$$

where $TD(i,j)$ is the transformed divergence between classes i and j and $D(i,j)$ is the divergence between classes i and j :

$$D(i,j) = 0.5 \times \mathbf{T}[\mathbf{M}(i) - \mathbf{M}(j)] \times [\mathbf{InvS}(i) + \mathbf{InvS}(j)] \times [\mathbf{M}(i) - \mathbf{M}(j)] \\ + 0.5 \times \text{Trace}[\mathbf{InvS}(i) \times \mathbf{S}(j) + \mathbf{InvS}(j) \times \mathbf{S}(i) - 2 \times \mathbf{I}] \quad (6)$$

where $\mathbf{M}(i)$ is the mean vector of class i , where the vector has Nchannel elements (Nchannel is the number of channels used), $\mathbf{S}(i)$ is the covariance matrix for class i , which has Nchannel \times Nchannel elements, $\mathbf{InvS}(i)$ is the inverse of matrix $\mathbf{S}(i)$, $\text{Trace}[\]$ is the trace of matrix (sum of diagonal elements), $\mathbf{T}[\]$ is the transpose of the matrix and \mathbf{I} is the identity matrix.

TD is an empirical measure for separability analysis that measures real values between 0 and 2, where '0' indicates complete overlap between the signatures of two

Table 1. Spectral separability analysis among eight change classes using transformed divergence (TD) before and after atmospheric correction.

Class	Class							
	1	2	3	4	5	6	7	8
Before atmospheric correction								
1		1.89	1.87	2.00	1.09	1.79	1.64	1.71
2	1.89		1.56	1.21	1.99	1.84	2.00	1.44
3	1.87	1.56		1.99	1.56	2.00	2.000	2.00
4	2.00	1.21	1.99		2.00	1.97	1.98	1.95
5	1.09	1.99	1.56	2.00		1.90	1.87	2.00
6	1.79	1.84	2.00	1.97	1.90		1.91	2.00
7	1.64	2.00	2.00	1.98	1.87	1.91		1.94
8	1.71	1.44	2.00	1.95	2.00	2.00	1.94	
After atmospheric correction								
1		1.99	2.00	2.00	2.00	1.99	1.91	2.00
2	1.99		1.68	1.92	2.00	1.86	1.96	1.99
3	2.00	1.68		2.00	1.85	2.00	1.94	2
4	2.00	1.92	2.00		1.96	2.00	2.00	2.00
5	2.00	2.00	1.85	1.96		2.00	2.00	1.97
6	1.99	1.89	2.00	2.00	2.00		1.990	2.00
7	1.91	1.96	1.94	2.00	2.00	1.99		2.00
8	2.00	1.99	2.00	2.00	1.97	2.00	2.00	

classes and '2' indicates a complete separation between the two classes (Swain and Davis 1978). These measures are monotonically related to classification accuracies. TD is calculated from the means and covariance matrices of each training class. It is a measure of the statistical distance between training group pairs of interest and provides information on their separability (Metternicht and Zinck 1998). It can be considered as an *a priori* estimate of the likelihood of correct classification between groups of different feature combinations. Table 1 shows the spectral separability among eight change classes using TD before and after atmospheric correction. It is evident from the table that atmospheric correction to the satellite data results in increased divergence values for all land use/land cover features, indicating better separability between features after atmospheric correction.

Figure 8 shows burnt areas as yellow colour patches overlaid on the corresponding IRS-P6 AWiFS FCC before and after atmospheric correction using the 6S code. It is clear from figure 8 that there is considerable misclassification between deciduous forests and burnt areas before the atmospheric corrections, leading to overestimation of the burnt areas. We also compared the different atmospheric correction algorithms, namely the COST model, the ATCOR model and the 6S code, for burnt area mapping over the region. Table 2 summarizes the burnt area estimates (in km²) before and after atmospheric correction using the different algorithms. Comparison of the burnt area estimates before and after atmospheric correction reveals that the fire-damaged areas are substantially different, with the total area classified as burnt on the uncorrected image extending to 1216.01 km² whereas on the corrected images it reached only 309.46 km² for the 6S code corrections, 356.35 km² for the ATCOR model corrections and 519.23 km² for the COST model corrections. This represents a reduction of approximately 906.64, 859.66 and 696.78 km², respectively (Gitas and Devereux 2006). The analysis reveals that the 6S code showed significant reduction in

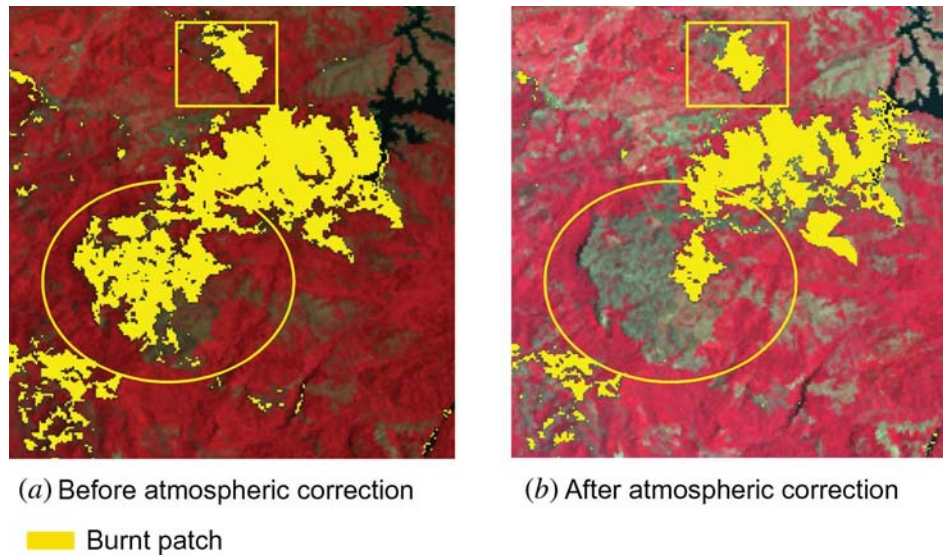


Figure 8. Classified image of AWiFS 19 March 2004 data (a) before and (b) after atmospheric correction.

Table 2. Burnt area statistics.

	Before atmospheric correction	COST model	ATCOR model	6S code
Burnt area (in km ²)	1216.01	519.23	356.35	309.46

burnt area estimates, followed by the ATCOR and COST models. Examination of the data reveals that most of the improvement in performance was due to increased separability between features after the atmospheric correction.

5. Conclusions

In the present study, DMSP-OLS and AWiFS data obtained during the fire season over Kerala State, India, were analysed. The information derived from multi-satellite data sets was compared and validated with ground observations. The results of the study show that DMSP-OLS-derived data are in good agreement with ground observations and multi-satellite data observations. However, the accuracy of the fire counts derived from the satellite data could be improved by using a forest area mask that would help in reducing errors as it would eliminate fire pixels falling outside the forest regions. As the DMSP-OLS pixel covers a ground area of 2.7 km, there is a high likelihood of fire occurrence within that pixel on subsequent days, which accordingly adds to fire counts estimated from DMSP data sets. The information, coupled with moderate/high-resolution data sets, provides a handle for effective monitoring of forest fires in a continuous manner. The combined use of DMSP-OLS MODIS and AWiFS data provides increased observation frequency for effective fire monitoring over this region. As the worst forest fires are those that go on from one day to the next, the DMSP provides a valuable indication of the fires that have burned into the night.

This is key information for use in managing and fighting fires. Atmospheric corrections to satellite datasets reduce the misclassification of burnt areas and help to increase the accuracy of burnt area mapping.

Acknowledgements

We are grateful to the Director and Deputy Director (RS&GIS-AA), NRSC, Hyderabad for their encouragement and ISRO-EOAM for funding support. We thank the officials of the Kerala Forest Department, and Dr. T.R. Kiran Chand and Biswadip Gharai for their help at various stages of this work.

References

- BADARINATH, K.V.S., KHAROL, S.K. and KIRAN CHAND, T.R., 2007, Use of satellite data to study the impact of forest fires over the northeast region of India. *IEEE Geoscience and Remote Sensing Letters*, **4**, pp. 485–489.
- BERK, A., BERNSTEIN, L.S. and ROBERTSON, D.C., 1989, *MODTRAN: A Moderate Resolution Model for LOWTRAN 7*. GL-TR-89-0122 (Bedford, MA: Phillips Laboratory, Hanscom AFB).
- CHAVEZ JR, P.S., 1996, Image-based atmospheric corrections – revisited and improved. *Photogrammetric Engineering and Remote Sensing*, **62**, pp. 1025–1036.
- CRUTZEN, P.J. and ANDREAE, M.O., 1990, Biomass burning in the tropics: impact on atmospheric chemistry and biogeochemical cycles. *Science*, **250**, pp. 1669–1678.
- DOZIER, J., 1981, A method for satellite identification of surface temperature fields of subpixel resolution. *Remote Sensing of Environment*, **11**, pp. 221–229.
- DWYER, E., GREGOIRE, J.M. and MALINGREAU, J.P., 1998, A global analysis of vegetation fires using satellite images: spatial and temporal dynamics. *Ambio*, **27**, pp. 175–181.
- ELVIDGE, C.D., BAUGH, K.E., KIHN, E.A., KROEHL, H.W. and DAVIS, E.R., 1997, Mapping of city lights using DMSP Operational Linescan System data. *Photogrammetric Engineering and Remote Sensing*, **63**, pp. 727–734.
- ELVIDGE, C.D., NELSON, I., HOBSON, V.R., SAFRAN, J. and BAUGH, K.E., 2001, Detection of fires at night using DMSP-OLS data. In *Global and Regional Vegetation Fire Monitoring from Space*, F.J. Ahern, J.G. Goldammer and C.O. Justice (Eds.), pp. 125–144 (Amsterdam, The Netherlands: SPB Academic Publishing).
- FEARNSIDE, P.M., 2000, Global warming and tropical land-use change: greenhouse gas emissions from biomass burning, decomposition and soils in forest conversion, shifting cultivation and secondary vegetation. *Climate Change*, **46**, pp. 115–158.
- FRENCH, N.H., KASISCHKE, E.S. and WILLIAMS, D.G., 2003, Variability in the emission of carbon-based trace gases from wildfire in the Alaskan boreal forest. *Journal of Geophysical Research*, **108**, p. 8151.
- GIGILIO, L., DESCLOITRES, J., JUSTICE, C.O. and KAUFMAN, Y.J., 2003, An enhanced contextual fire detection algorithm for MODIS. *Remote Sensing of Environment*, **87**, pp. 273–282.
- GITAS, I.Z. and DEVEREUX, B.J., 2006, The role of topographic correction in mapping recently burned Mediterranean forest areas from Landsat TM images. *International Journal of Remote Sensing*, **27**, pp. 41–54.
- GOVAERTS, Y., PEREIRA, J.M., PINTY, B. and MOTA, B., 2002, Impact of fires on surface albedo dynamics over the African continent. *Journal of Geophysical Research*, **107**, pp. 4629–4633.
- GUANTER, L., ESTELLES, V. and MORENO, J., 2007a, Spectral calibration and atmospheric correction of ultra-fine spectral and spatial resolution remote sensing data: application to CASI-1500 data. *Remote Sensing of Environment*, **109**, pp. 54–65.
- GUANTER, L., SANPEDRO, G., CARMEN, M.D. and MORENO, J., 2007b, A method for the atmospheric correction of ENVISAT/MERIS data over land targets. *International Journal of Remote Sensing*, **28**, pp. 709–728.

- HAO, W.M. and LIU, M.H., 1994, Spatial and temporal distribution of biomass burning. *Global Biogeochemical Cycles*, **8**, pp. 495–503.
- HAO, W.M., WARD, D.W., OLBUR, G. and BAKER, S.P., 1996, Emissions of CO₂, CO, and hydrocarbons from fires in diverse African savanna ecosystems. *Journal of Geophysical Research*, **101**, pp. 23577–23584.
- KAUFMAN, Y.J., HOBBS, P.V., KIRCHOFF, V.W., ARTAXO, P., REMER, L.A., HOLBEN, B.N., KING, M.D., WARD, D.E., PRINS, E.M., LONGO, K.M., MATTOS, L.F., NOBRE, C.A., SPHINIRNE, J.D., JI, Q., THOMPSON, A.M., GLEASON, J.F., CHRISTOPHER, S.A. and TSAY, S.-C., 1998a, Smoke, Clouds and Radiation–Brazil (SCAR-B) experiment. *Journal of Geophysical Research*, **103**, pp. 31783–31808.
- KAUFMAN, Y.J., JUSTICE, C.O., FLYNN, L.P., KENDALL, J.D., PRINS, E.M., GIGLIO, L., WARD, D.E., MENZEL, W.P. and SETZER, A.W., 1998b, Potential global fire monitoring from EOS-MODIS. *Journal of Geophysical Research*, **103**, pp. 32215–32238.
- KIRAN CHAND, T.R., BADARINATH, K.V.S., KRISHNA PRASAD, V., MURTHY, M.S.R., ELVIDGE, C.D. and TUTTLE, B.T., 2006, Monitoring forest fires over the Indian region using Defense Meteorological Satellite Program–Operational Linescan System nighttime satellite data. *Remote Sensing of Environment*, **103**, pp. 165–178.
- KNEIZYS, F.X., SHETTLE, E.P., ABREU, L.W., CHETWYND, J.H., ANDERSON, G.P., GALLERY, W.O., SELBY, J.E.A. and CLOUGH, S.A., 1988, *User's Guide to LOWTRAN 7*. Environmental Research Report ERP No. 1010 (Bedford, MA: Air Force Geophysics Laboratory, Hanscom AFB).
- LIANG, S., FANG, H. and CHEN, M., 2001, Atmospheric correction of Landsat ETM+ land surface imagery: I. Methods. *IEEE Transactions on Geoscience and Remote Sensing*, **39**, pp. 2490–2498.
- LU, D., MAUSEL, P., BRONDIZIO, E. and MORAN, E., 2002, Assessment of atmospheric correction methods for Landsat TM data applicable to Amazon basin LBA research. *International Journal of Remote Sensing*, **23**, pp. 2651–2671.
- LYAPUSTIN, A.I. and KAUFMAN, Y.J., 2001, The role of adjacency effect in the remote sensing of aerosol over the land. *Journal of Geophysical Research*, **106**, pp. 11909–11916.
- MAHINY, A.S. and TURNER, B.J., 2007, A comparison of four common atmospheric correction methods. *Photogrammetric Engineering and Remote Sensing*, **73**, pp. 361–368.
- MASEK, J.G., VERMOTE, E.F., SALEOUS, N.E., WOLFE, R., HALL, F.G., HUENNRICH, K.F., GAO, F., KUTLER, J. and LIM, T.K., 2006, A Landsat surface reflectance dataset for North America, 1990–2000. *IEEE Geoscience and Remote Sensing Letters*, **3**, pp. 68–72.
- MATSON, M., SCHNEIDER, S.R., ALDRIDGE, A. and SACHEL, B., 1984, *Fire Detection Using the NOAA Series Satellites*. NOAA-NESS Technical Report 7 (Washington, DC: NOAA).
- MATSON, M., STEPHENS, G. and ROBINSON, J., 1987, Fire detection using data from the NOAA-N satellites. *International Journal of Remote Sensing*, **8**, pp. 961.
- METTERNICHT, G.I. and ZINCK, J.A., 1998, Evaluating the information content of JERS-1 SAR and Landsat TM data for discrimination of soil erosion features. *ISPRS Journal of Photogrammetry and Remote Sensing*, **53**, pp. 143–153.
- PRASAD, V.K., BADARINATH, K.V.S. and ANURADHA, E., 2008, Spatio-temporal analysis of fire events in India: implications for environmental conservation. *Journal of Environmental Planning and Management*, **51**, pp. 817–832.
- RAHMAN, H. and DEDIEU, G., 1994, SMAC: a simplified method for atmospheric correction of satellite measurements in the solar spectrum. *International Journal of Remote Sensing*, **15**, pp. 123–143.
- REID, J.S., ECK, T.F., CHRISTOPHER, S.A., KOPPMANN, R., DUBOVIK, O., ELEUTERIO, D.P., HOLBEN, B.N., REID, E.A. and ZHANG, J., 2005, A review of biomass burning emissions. Part III: Intensive optical properties of biomass burning particles. *Atmospheric Chemistry and Physics*, **5**, pp. 827–849.

- RICHTER, R., SCHLAPFER, D. and MULLER, A., 2006, An automatic atmospheric correction algorithm for visible/NIR imagery. *International Journal of Remote Sensing*, **27**, pp. 2077–2085.
- ROY, D.P., JIN, Y., LEWIS, P.E. and JUSTICE, C.O., 2005, Prototyping a global algorithm for systematic fire-affected area mapping using MODIS time series data. *Remote Sensing of Environment*, **97**, pp. 137–162.
- SEI, A., 2007, Analysis of adjacency effects for two Lambertian half-spaces. *International Journal of Remote Sensing*, **28**, pp. 1873–1890.
- SHARMA, A.R., BADARINATH, K.V.S. and ROY, P.S., 2009, Comparison of ground reflectance measurement with satellite derived atmospherically corrected reflectance: a case study over semi arid landscape. *Advances in Space Research*, **43**, pp. 56–64.
- STEFANOV, W.L., RAMSEY, M.S. and CHRISTENSEN, P.R., 2001, Monitoring urban land cover change: an expert system approach to land cover classification of semiarid to arid urban centers. *Remote Sensing of Environment*, **77**, pp. 173–185.
- STROEVE, J.N. and STEFFEN, K., 1997, Comparison of AVHRR-derived and in situ surface albedo over the Greenland ice sheet. *Remote Sensing of Environment*, **62**, pp. 262–276.
- SWAIN, P.H. and DAVIS, S.M. (Eds.), 1978, *Remote Sensing: The Quantitative Approach* (New York: McGraw-Hill).
- TACHIRI, K., 2005, Calculating NDVI for NOAA/AVHRR data after atmospheric correction for extensive images using 6S code: a case study in the Marsabit District, Kenya. *ISPRS Journal of Photogrammetry and Remote Sensing*, **59**, pp. 103–114.
- TANRE, D., DEROO, C., DAHAUT, P., HERMAN, M. and MORCRETTE, J.J., 1990, Description of a computer code to simulate the satellite signal in the solar spectrum: the 5S code. *International Journal of Remote Sensing*, **11**, pp. 659–688.
- VERMOTE, E.F. and SALEOUS, N.Z., 2006, Operational atmospheric correction of MODIS visible to middle infrared land surface data in the case of an infinite Lambertian target. In *Earth Science Satellite Remote Sensing, Science and Instruments*, J. Qu, W. Gao, M. Kafatos, R.E. Murphy and V.V. Salomonson (Eds.), vol. 1, pp. 123–153 (Berlin, Heidelberg: Springer).
- VERMOTE, E.F., SALEOUS, N.Z. and JUSTICE, C.O., 2002, Atmospheric correction of MODIS data in the visible to middle infrared: first results. *Remote Sensing of Environment*, **83**, pp. 97–111.
- VERMOTE, E.F., TANRE, D., DEUZE, J.L., HERMAN, M. and MORCRETTE, J.J., 1997, Second Simulation of the Satellite Signal in the Solar Spectrum, 6S: an overview. *IEEE Transactions on Geoscience and Remote Sensing*, **35**, pp. 675–686.
- WU, J., WANG, D. and BAUER, M.E., 2005, Image-based atmospheric correction of QuickBird imagery of Minnesota cropland. *Remote Sensing of Environment*, **99**, pp. 315–325.
- ZHAO, W., TAMURA, M. and TAKAHASHI, H., 2001, Atmospheric and spectral corrections for estimating surface albedo from satellite data using 6S code. *Remote Sensing of Environment*, **76**, pp. 202–212.